COMPARISON BETWEEN PHYSICAL AND NUMERICAL MODELS OF THE VELOCITY MEASUREMENT IN THE LATERAL CHANNEL OF THE ANCOA RESERVOIR

F. NEGRETE[1], J. COTRONEO[2] , L. ZAMORANO[3] , C. OSORIO[4] , Y. NIÑO[5] & A. TAMBURRINO[6]

[1,2,3,4] Instituto Nacional de Hidráulica, Santiago, Chile,
felipenegrete@inh.cl, jaimecotroneo@inh.cl, luiszamorano@inh.cl, camilaosorio@inh.cl

[5,6] Departamento de Ingeniería Civil and Advanced Mining Technology Center - Universidad de Chile, Chile
ynino@ing.uchile.cl, atamburr@ing.uchile.cl

ABSTRACT

Velocity measurements with Acoustic Doppler Velocimeter (ADV) in the collector channel of Ancoa Reservoir's physical model are contrasted with LES numerical simulation results. In order to evaluate the accuracy and applicability of the numerical model in highly turbulent flows, times series of velocity fields, Reynolds stress ($\overline{u'w'}$) and energy spectral density are compared. LES calculations were developed in OpenFOAM free software and a wall adapting local eddy viscosity (WALE) model was used. The ADV data have been filtered in order to get rid of the spikes in the velocity signal due to the air bubble presence. The analysis was carried out for a constant discharge of 761 m^3/s in prototype, corresponding to floods with a return period of 1.000 years. The results show that LES numerical model predicts well the average turbulent flow variables, but those associated with turbulent fluctuations are not satisfactory.

Keywords: Acoustic Doppler Velocimeter (ADV), LES, OpenFOAM, physical model

1 INTRODUCTION

In the field of hydraulic design, complex situations are usually validated through physical models. However, due to the high cost of laboratory experiments and the current computational advance, researchers have attempted to use numerical simulation along with physical modeling (Dehdar-behbahani & Parsaie, 2016). Recently, the tendency to use physical and numerical models jointly can be applied in different ways. For instance, it can be used in the early design stages, where numerical modeling can provide boundary conditions for physical models, or in later stages, as a design tool to explore several solution alternatives. This kind of modeling is referred to by some authors as hybrid modeling or composite modeling (Kamphuis 1995, Kamphuis 1996 and Ettema et al. 2000). A common factor to this approach is the need to validate CFD models with the data collection of the physical models (Hager & Boes, 2014).

In this context of hybrid modeling, the National Institute of Hydraulics in Chile (INH) and the University of Chile, have developed a study to improve the design of the spillway of the Ancoa reservoir, located almost 300 km south of Santiago. To do this, a physical model of the existing structure was built at 1:40 Froude scale. Also, a numerical model was used to test different alternatives in order to decrease the high flow agitation in the collector channel. To implement the numerical model, the open source OpenFOAM software was used. In particular, the solver interFoam can handle incompressible two-phase flow problems by applying an interface capturing technique based on a modified volume of fluid (VoF) approach. On the treatment of turbulence, the Reynolds average equations (RANS) were initially used, but early comparisons between the physical and numerical model showed that the free surface in the collector channel was not well reproduced by RANS, making it necessary to improve the numerical model. For this reason, an increase in the grid resolution and a different treatment of the turbulence was implemented. In this case, the idea was to capture the flow separation in the lateral spillway in a better way than RANS, using a Large Eddy Simulation (LES) approach (Spalar 2009, Rodi et al. 2013 and Thorsten 2014). Finally, the numerical model was in agreement with the punctual values of the surface elevation (Negrete et al., 2015).

Later, a more rigorous analysis of time series of hydrodynamic parameters, surface elevation and pressure, was made to evaluate and validate the numerical model. The results showed a good agreement, in particular, the free surface showed a better result than the pressure, which had a range of error in the average pressure of 3-18% (Negrete et al., 2016). Similar results are obtained by other authors in similar cases, for example, Sánchez-Cordero et al. (2018) who used OpenFoam for the analysis of a dam-break in a 3D numerical model, using VOF method and LES. In similar applications, there are no results related to the velocity in order to make a comparison.

In this study, a comparison between velocity measurements taken with an Acoustic Doppler Velocimeter (ADV) and the results of the numerical model with LES and WALE subgrid model is shown. ADV is an instrument capable of reporting instantaneous and mean values of water velocities in three directions. However, ADV measurements are altered by several factors that negatively influence the data recorded by the instrument, whose effect is increased in highly aerated and turbulent flows as in the present study. For instance, the data are contaminated by spikes, which are random outliers that can occur due to the interference of previous pulses reflected from flow boundaries or due to the presence of bubbles, sediments, etc. In order to clean up the contaminated data measured by the ADV, the methodology proposed by Goring and Nikora (2002), specialized for highly aerated flows, has been used.

2 METHODS

The two tools used in the study, whose results are shown in this paper, are physical and numerical models. A brief review of each of them is shown below.

2.1 Physical model

The physical model was built in 1:40 scale following the Froude similarity criterion in an undistorted model. General layout and the turbulent flow generated in the collector channel of the physical model are shown in Figure 1 and Figure 2, respectively. Besides, Table 1 shows the values of the main features of the spillway and their corresponding values in the physical model.

Figure 1. General layout of the physical model in laboratory.

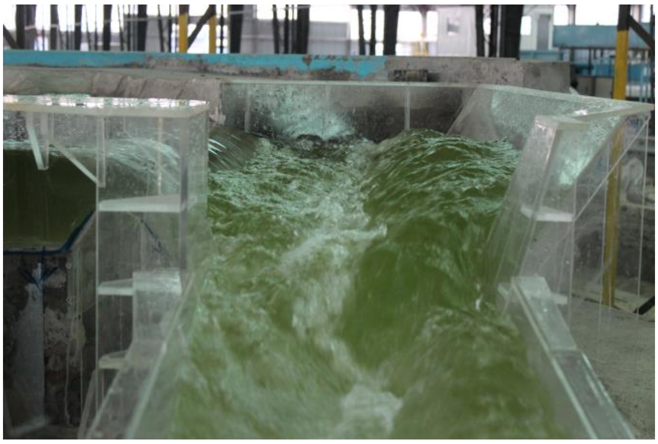

Figure 2. View of the turbulent flow in the collector channel.

Table 1. Main features of the spillway.

	Unit	Prototype	Model (1:40)
Design Head on crest of Ogee spillway	m	4.015	0.100
Length of the collector channel	m	45.000	1.130
Minimum width of the collector channel	m	10.000	0.250
Maximum width of the collector channel	m	12.000	0.300
Discharge (Return period of 1.000 years)	m^3/s	761	0.075

2.2 Numerical model

In this study, the computational tool used is the open-source CFD software OpenFOAM v1712. In particular, the solver Interfoam was used, which can deal with two incompressible (air and water), isothermal, immiscible fluids, using a VOF (volume of fluid) phase-fraction based interface capturing approach. In all cases, in order to know where the interphase between the two fluids (air and water) is located, a value of α = 0.5 was used in post-processed data, where α is the so-called indicator field introduced for convenience, which takes the value 0 in air and 1 in water.

For the turbulence modeling, a Large Eddy Simulation (LES) approach is considered. Although many different SGS models exist in OpenFOAM, the wall adapting local eddy viscosity (WALE) model was selected because it works better close to the walls than Smagorinsky SGS model. In particular, it is able to model the laminar to turbulence transition (Bin and Xian-Wu, 2013), and the computational cost is not high.

The domain of the model is shown in Figure 3. It is approximately a box of 11m x 5m x 2m. The mesh has 3.282.412 cells. The cell resolution is variable in the domain, with the smallest edges values in the walls of the study zone (0.6 mm). This was done to achieve a distance in wall units y^+ equal to 6 or less.

2.3 ADV Measurements

ADV used in the measurement works with an acoustic frequency of 10 MHz and its sampling was set in 150 Hz. Velocities were measured in three cross-sections of the collector channel (P1, P2 y P3 in Figure 4). In each profile, the velocity was recorded in 26 points.

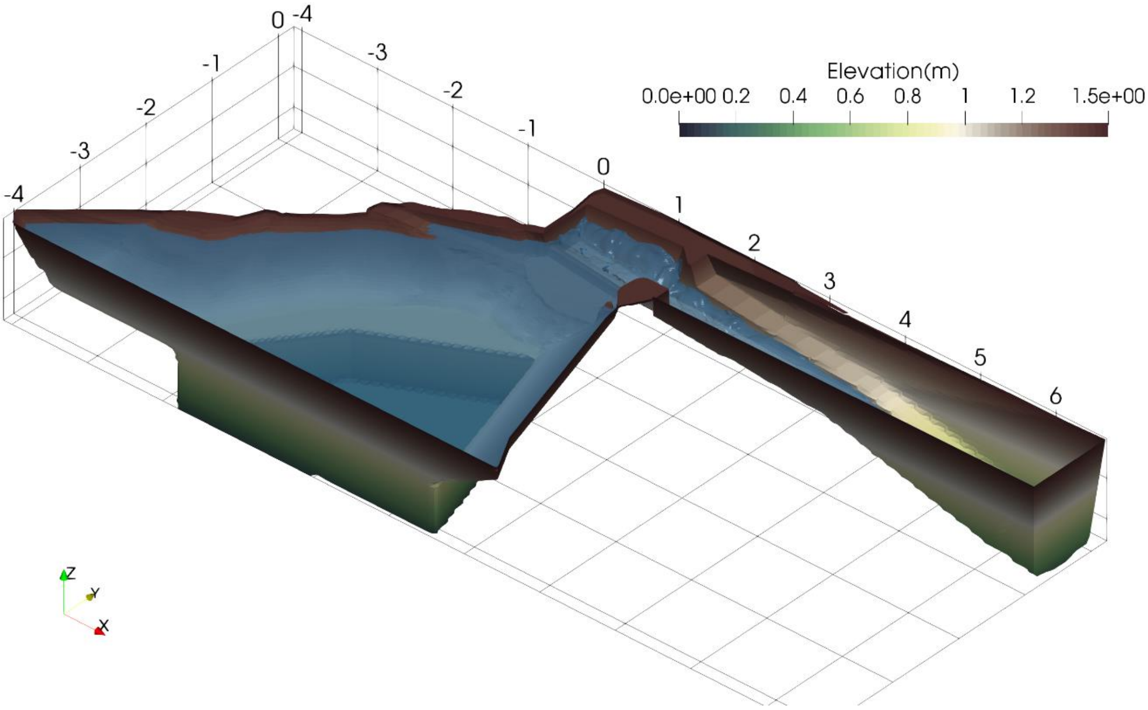

Figure 3. Sketch of numerical model.

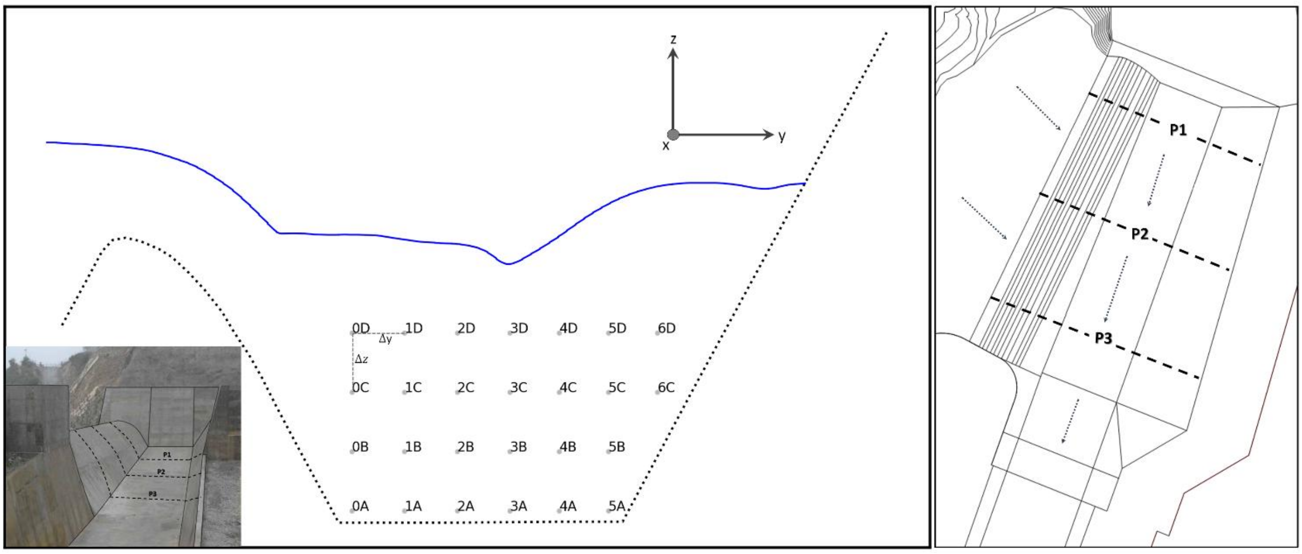

Figure 4. Measured points in transversal profile. Both vertical (Δz) and horizontal (Δy) spacing equals 5cm. The notation is the one used in the comparison between physical and numerical model.

3 RESULTS AND DISCUSSION

The velocities recorded in the locations shown in Figure 4 are used to compare the differences between the physical and the numerical models. The following shows the comparison of time-series, time-averaged velocity, Reynolds stress and energy density spectrum.

3.1 Comparison of time-series and vector velocity

First of all, it is important to evaluate the temporal fluctuation of the velocities at any point of the collector channel. In order to compare both, physical and numerical models, time series plots at location 5D are shown in Figure 5. ADV measurements in the physical model show the great magnitude of the velocity fluctuations in the collector channel, although they are affected by the presence of air bubbles. Furthermore, since the calculated results of the numerical simulation pass through a filter, the LES model, the same is done with ADV data and a simple moving average to 5 Hz frequency is also presented in these plots (Figure 5). Then, it is possible to see a similarity in the fluctuations of velocity in the physical and the numerical model.

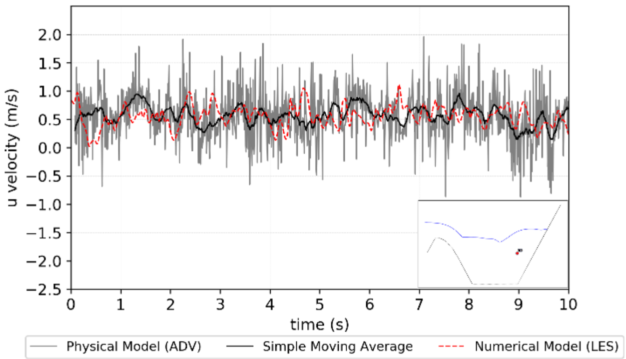

(a)

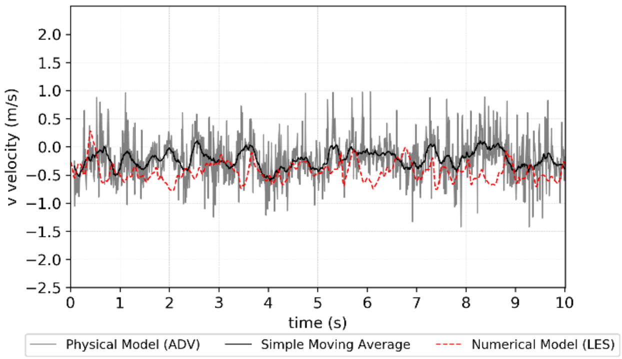

(b)

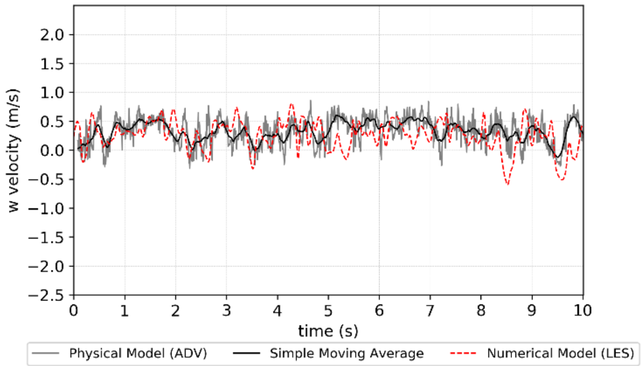

(c)

Figure 5. Comparison of velocity time series between physical and numerical models at location 5D, profile P2. Corresponding to (a) u-longitudinal component, (b) v-transverse component and (c) w-vertical component.

Additionally, in order to compare the velocity mean behavior as a vector, that is, also visualizing its y-z direction, Figure 6 shows a vector map in a transversal profile of the collector channel for the physical and numerical model. Here it is clearly seen how the numerical model is able to reproduce the vortex that is generated in the channel.

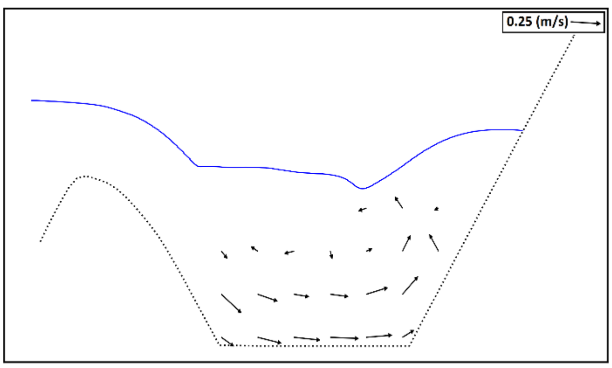

(a)

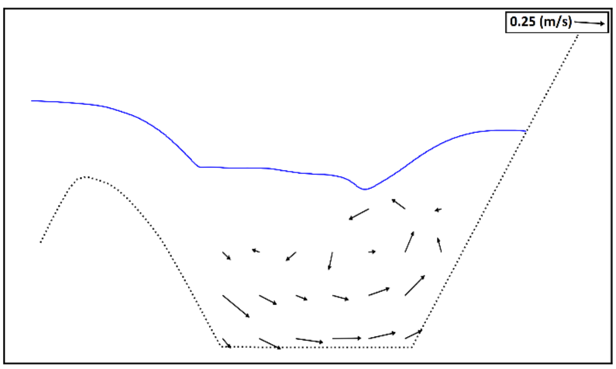

(b)

Figure 6. Vector map of the mean velocities in cross section P2 for (a) Physical model and (b) Numerical model.

In Figure 6, it is observed that some vectors are not of the same order of magnitude in the physical and numerical models. This difference in value is due to the fact that the ADV captures the changes of direction of the resulting y-z velocities, and the numerical model does not. In Figure 7a represents the “wind rose” of the point 2C. The great variability in time of the velocity vector can be observed for the case of the physical model, but the numerical model shows less variability over time (Figure 7b).

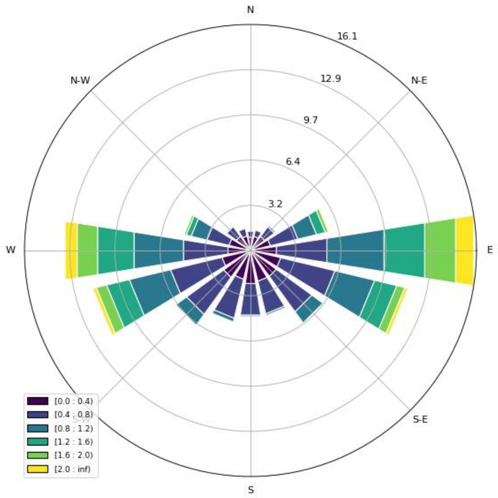

(a)

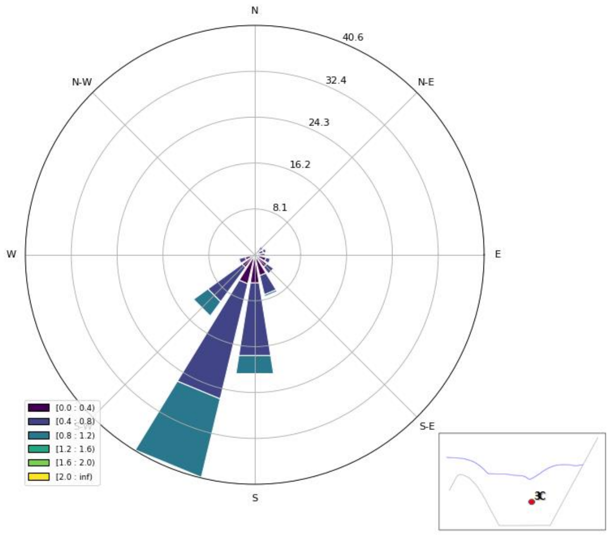

(b)

Figure 7. Wind rose at point 3C, cross section P2 for (a) Physical model and (b) Numerical model.

3.2 Comparison of time-averaged velocity

Figure 8 shows the time-averaged velocity in each of the main directions ($\bar{u}$, $\bar{v}$ and $\bar{w}$) for both the physical and the numerical models. It is clear that, in general, the average values of the velocity show a very good correlation between physical and numerical models. Although, for the velocity in x-direction ($\bar{u}$), there are some locations that show high discordance between both models (6D, 6C and 4D). These locations are right on the vortex (Figure 2 and Figure 6), with a high presence of bubbles, and therefore, neither the numerical model nor the physical model present reliable data. Table 2, Table 3 and Table 4 shows the magnitude of time-averaged velocity in the longitudinal direction ($\bar{u}$), transverse direction ($\bar{v}$) and vertical direction ($\bar{w}$), respectively, together with its RMS values calculated for both numerical and physical models. It shows better similarity in the mean values of the velocity, which contrasts with the difference in the values of the fluctuations. Although the data in Table 2 is for cross section P1, the same behavior is observed in P2 and P3.

Table 2. Magnitude of time-averaged longitudinal velocity ($\bar{u}$) and its rms values in cross section P1.

	Physical Model		**Numerical Model**			**Physical Model**		**Numerical Model**	
Location	$\bar{u}\ (\frac{m}{s})$	$rms\ (\frac{m}{s})$	$\bar{u}\ (\frac{m}{s})$	$rms\ (\frac{m}{s})$	**Location**	$\bar{u}\ (\frac{m}{s})$	$rms\ (\frac{m}{s})$	$\bar{u}\ (\frac{m}{s})$	$rms\ (\frac{m}{s})$
0A	0.195	0.232	0.307	0.124	**4B**	0.315	0.349	0.301	0.179
1A	0.216	0.109	0.284	0.121	**0C**	0.161	0.332	0.229	0.111
2A	0.208	0.100	0.305	0.097	**1C**	0.218	0.265	0.240	0.156
3A	0.199	0.138	0.303	0.118	**2C**	0.165	0.361	0.194	0.173
4A	0.192	0.155	0.283	0.137	**3C**	0.078	0.540	0.149	0.166
5A	0.172	0.161	0.219	0.200	**4C**	0.089	0.602	0.259	0.187
0B	0.132	0.244	0.219	0.057	**5C**	0.249	0.364	0.348	0.182
1B	0.203	0.255	0.248	0.116	**6C**	0.067	0.448	0.061	0.180
2B	0.212	0.314	0.284	0.180	**5D**	0.054	0.604	0.102	0.171
3B	0.236	0.396	0.259	0.174	**6D**	0.159	0.289	0.024	0.138

Table 3. Magnitude of time-averaged transverse velocity ($\bar{v}$) and its rms values in cross section P1.

	Physical Model		Numerical Model			Physical Model		Numerical Model	
Location	$\bar{v}\ (\frac{m}{s})$	$rms\ (\frac{m}{s})$	$\bar{v}\ (\frac{m}{s})$	$rms\ (\frac{m}{s})$	**Location**	$\bar{v}\ (\frac{m}{s})$	$rms\ (\frac{m}{s})$	$\bar{v}\ (\frac{m}{s})$	$rms\ (\frac{m}{s})$
0A	0.017	0.238	0.294	0.174	**4B**	0.490	0.347	0.536	0.259
1A	0.653	0.282	0.615	0.213	**0C**	0.561	0.445	0.142	0.176
2A	0.975	0.153	1.068	0.186	**1C**	-0.068	0.304	-0.032	0.201
3A	1.013	0.205	1.138	0.226	**2C**	-0.257	0.396	-0.146	0.223
4A	0.938	0.234	1.019	0.285	**3C**	-0.245	0.560	-0.187	0.225
5A	0.462	0.283	0.402	0.301	**4C**	-0.084	0.640	-0.006	0.198
0B	0.587	0.411	0.973	0.103	**5C**	0.107	0.344	0.176	0.177
1B	0.754	0.394	0.838	0.199	**6C**	0.108	0.533	-0.146	0.155
2B	0.468	0.397	0.498	0.316	**5D**	-0.252	0.552	-0.493	0.132
3B	0.337	0.413	0.412	0.285	**6D**	-0.206	0.275	0.008	0.159

Table 4. Magnitude of time-averaged vertical velocity ($\bar{w}$) and its rms values in cross section P1.

	Physical Model		Numerical Model			Physical Model		Numerical Model	
Location	$\bar{w}\ (\frac{m}{s})$	$rms\ (\frac{m}{s})$	$\bar{w}\ (\frac{m}{s})$	$rms\ (\frac{m}{s})$	**Location**	$\bar{w}\ (\frac{m}{s})$	$rms\ (\frac{m}{s})$	$\bar{w}\ (\frac{m}{s})$	$rms\ (\frac{m}{s})$
0A	0.051	0.083	0.168	0.261	**4B**	0.061	0.222	0.086	0.224
1A	-0.260	0.060	-0.316	0.122	**0C**	-0.492	0.145	-0.141	0.115
2A	-0.104	0.055	-0.167	0.091	**1C**	0.025	0.185	-0.012	0.154
3A	-0.052	0.069	-0.042	0.101	**2C**	0.143	0.186	0.062	0.183
4A	0.023	0.084	0.113	0.110	**3C**	-0.086	0.222	-0.185	0.260
5A	0.233	0.076	0.149	0.115	**4C**	-0.010	0.237	-0.122	0.308
0B	-0.623	0.076	-0.743	0.051	**5C**	0.271	0.216	0.394	0.211
1B	-0.395	0.127	-0.405	0.105	**6C**	0.591	0.204	0.176	0.263
2B	-0.055	0.182	-0.077	0.128	**5D**	-0.033	0.229	0.037	0.252
3B	-0.044	0.231	-0.042	0.197	**6D**	0.432	0.180	-0.101	0.222

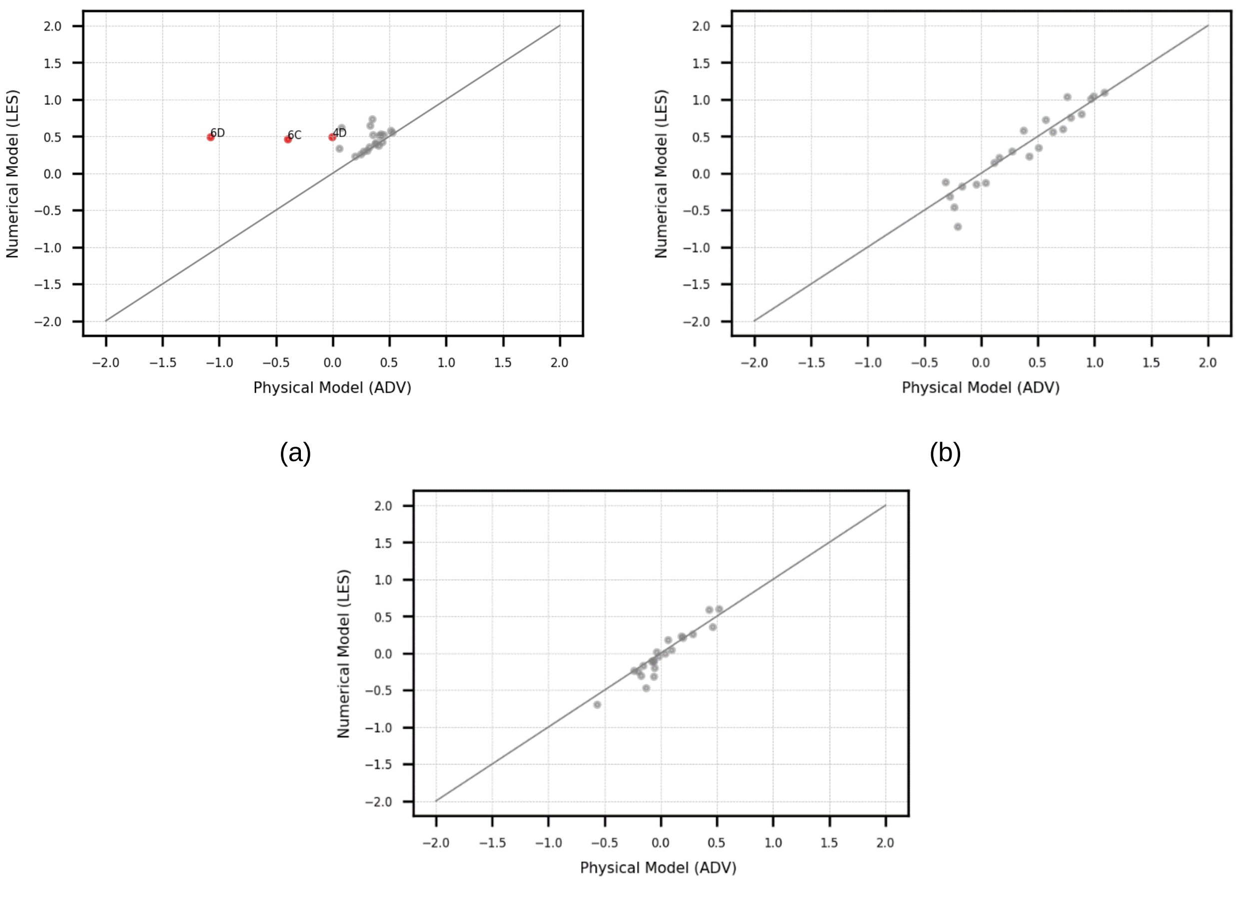

Figure 8. Magnitude of the time-averaged velocity in cross sections (a) P1 (b) P2 and (c) P3.

3.3 Reynolds stresses

In order to compare the Reynolds stress, $\overline{u'w'}$ is calculated in the physical and numerical models. Figure 9 shows the results for cross sections P1, P2 and P3. Red dots are considered invalid data since they are in the zone with a large presence of air bubbles. Despite this, points of low correlation between the numerical and physical model are observed, which is mainly due to the difference in the magnitude of the velocity fluctuations in the longitudinal direction (u') as shown in Figure 5a.

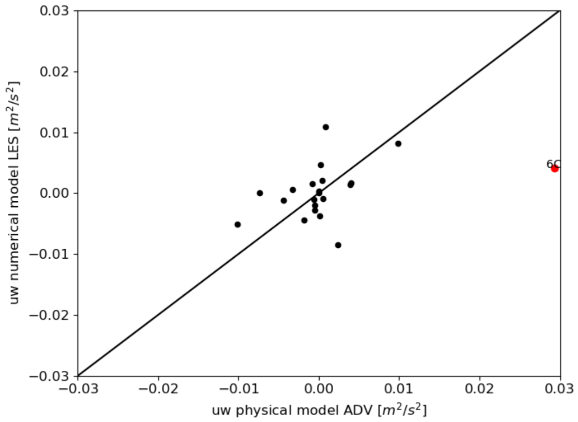

(a)

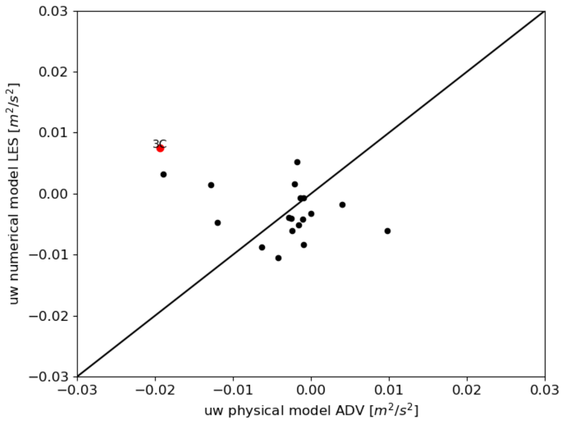

(b)

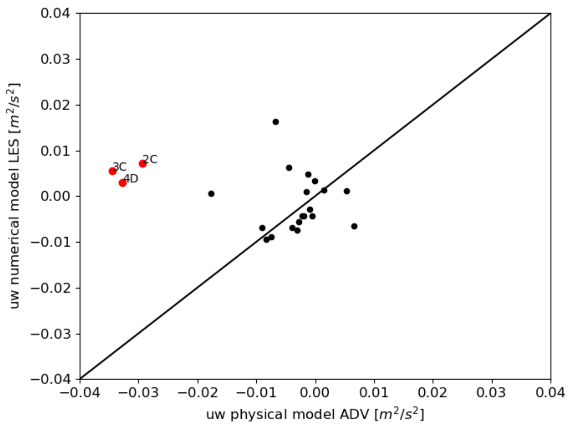

(c)

Figure 9. Stress $\overline{u'w'}$ (a) Transverse Profile P1 (b) cross section P1 and (c) cross section P3.

3.4 Energy density spectrum

The measured and computed power spectral densities of the velocities at location 3A of cross section P2 are presented in Figure 10. In the graphs, $f_{integral}$ corresponds to the frequency associated to the integral time, which is calculated by Eq. [1].

$$f_{integral} = \frac{1}{T_{integral}} \quad [1]$$

where,

$$T_{integral} = \frac{1}{N\sigma}\sum_{t=1}^{N-K}(u_t - \overline{u})(u_{t+1} - \overline{u}) \quad [2]$$

where, $T_{integral}$ is the integral time, N the numbers of data, σ the variance, u_t the velocity in the t-time and $\bar{u}$ the time-averaged velocity.

Besides, f_{LES} is the limit frequency for which the turbulent stresses are solved by the numerical model, that is, for frequencies lower than f_{LES} the model calculates, while for greater frequencies it is modeled.

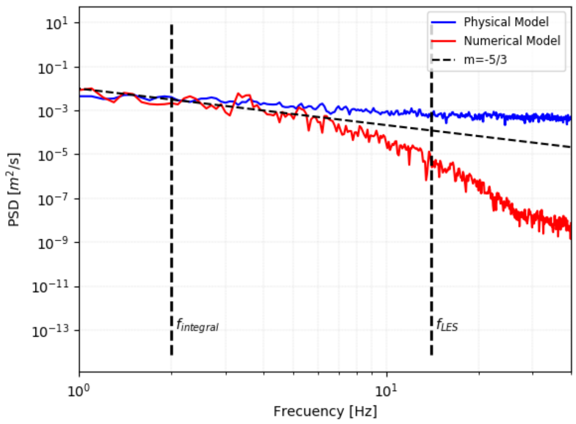

(a)

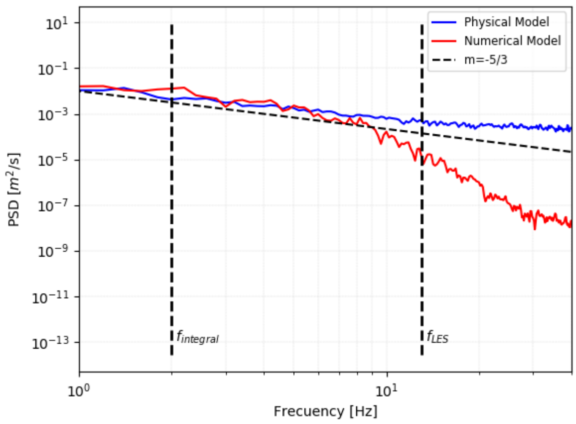

(b)

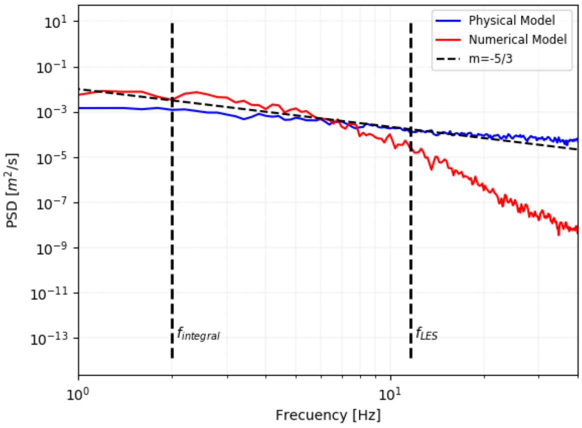

(c)

Figure 10. Energy Density Spectrum for (a) *u* velocity (b) *v* velocity and (c) *w* velocity.

In Figure 10 it is observed how the LES numerical model reproduces well the energy for the fluctuations of low energy, but not the high frequencies where the dissipative characteristic of the numerical model is evidenced.

4 CONCLUSIONS

To validate the results of the LES numerical model in a highly turbulent flow, like that of a collector channel, the velocity was measured with an ADV at several locations of the physical model of the spillway of the Ancoa reservoir. Different variables are compared between both, physical and numerical models, such as time series of the velocities, time-averaged velocities, Reynolds stress and power spectral density.

First, it has been shown that the LES numerical model accurately represents the average values of the velocity in all its directions. However, regarding the magnitude of the fluctuations in the longitudinal (u') and transverse directions (v'), an underestimation is observed. The fluctuations in the vertical direction are well modeled by LES. Additionally, the velocity field in the cross section of the collector channel is well reproduced by the numerical model, clearly identifying the vortex seen in the physical model. It is worth mentioning that the points located in the presence of many air bubbles, neither the ADV nor the numerical model give certainty of the results.

Regarding the Reynolds stress, there is not a good correlation between both models, which is considered a result of the discrepancy between the velocity fluctuation in the physical and LES models.

The comparison of the power spectral density shows that the fluctuations of low frequencies (higher energy) are very well represented in the LES numerical model. At higher frequencies, the dissipative characteristic of LES numerical model is observed.

Finally, the results of this study and that of Negrete et al. (2016) allow us to conclude that LES correctly reproduces the average hydrodynamic variables of the flow so that its use is valid for engineering designs. In contrast, LES does not accurately reproduces the variables associated with the flow turbulence, so if necessary, other analysis tools would be needed.

ACKNOWLEDGEMENTS

The authors thank the Ministry of Public Works of Chile for allowing use of the results of the study.

REFERENCES

Bin J. and Xian-Wu L. (2013). Three dimensional large eddy simulation and vorticity analysis of unsteady cavitating flow around a twisted hydrofoil. Journal of Hydrodynamics, 25(4), 501-519.
Dehdar-behbahani S. and Parsaie A. (2916). *Numerical modeling of flow pattern in dam spillway's guide wall. Case study: Balaroud dam, Iran.* Alexandria Engineering Journal, 55, 467-473.
Ettema R., Arndt R., Roberts P. and Wahl T. (2000). *Hydrauling modeling: Concepts and practice.* Reston, Virginia. American Society of Civil Engineers.
Hager W.H. and Boes R.M. (2014). *Hydraulic structures: a positive outlook into the future.* Journal of Hydraulic Research, 52 (3), 299-310.
Goring D.G. and Nikora V.I. and (2000). *Despiking Acoustic Doppler Velocimeter Data.* J. Hydraulic Eng, 128, 117-126.
Kamphuis J.W. (1995). *Composite modelling - an old tool in a new context.* Proceedings of the Congress International Association for Hydraulic Research,1.
Kamphuis J.W. (1996). *Physical modeling of coastal processes.* Advances in Coastal and Ocean Engineering, 79-114.
Negrete F., Cotroneo J., Zamorano L., Niño Y. and Tamburrino A. (2015). *Physical and numerical model of the flood spillway of the Ancoa reservoir, Maule Region. In Spanish.* XXII Congreso Chileno de Ingeniería Hidráulica, Santiago, Chile, 2015.
Negrete F., Cotroneo J., Zamorano L., Niño Y. and Tamburrino A. (2016). *Comparison between physical and numerical modeling in the flood spillway of the Ancoa reservoir, Chile. In Spanish.* XXVII Congreso Latinoamericano de Hidráulica, Lima, Perú, 2016.
Spalart P.R. (2009). *RANS modelling into a second century.* International Journal of Computational Fluid Dynamics, 23(4), 291-293.
Thorsten S. (2014). *Large-eddy simulation in hydraulics: Quo valids?* Journal of Hydraulic Research, 52(4), 441-452.
Rodi W., Constantinescu G. and Stoesser T. (2013). *Large-Eddy Simulations in Hydraulics.* EH Leiden. CRC Press/Balkema.
Sánchez-Cordero E. et al (2018). *3D numerical analysis of a dam-break using VOD method and LES turbulence model.* Ingeniería del Agua, 22(3), 167-176.